Stepwise Length Changes in Single Invertebrate Thick Filaments

Ekaterina M. Nagornyak, Felix A. Blyakhman, and Gerald H. Pollack
Department of Bioengineering, University of Washington, Seattle, Washington

ABSTRACT Previous experiments on thick filaments of the anterior byssus retractor muscle of *Mytilus* and the telson-levator muscle of *Limulus polyphemus* have shown large, reversible length changes up to 23% and 66% of initial length, respectively, within the physiological tension range. Using nanofabricated cantilevers and newly developed high-resolution detection methods, we investigated the dynamics of isolated *Mytilus* anterior byssus retractor muscle thick filaments. Single thick filaments were suspended between the tips of two microbeams oriented perpendicular to the filament axis: a deflectable cantilever and a stationary beam. Axial stress was applied by translating the base of the deflectable nanolever away from the stationary beam, which bent the nanolever. Tips of flexible nanolevers and stationary beam were imaged onto a photodiode array to track their positions. Filament shortening and lengthening traces, obtained immediately after the motor had imposed stress on the filament, showed steps and pauses. Step sizes were 2.7 nm and integer multiples thereof. Steps of this same size paradigm have been seen both during contraction of single sarcomeres and during active interaction between single isolated actin and myosin filaments, raising the question whether all of these phenomena might be related.

INTRODUCTION

In approaching the mechanism of motility and contraction, considerable attention has turned toward the elastic properties of the muscle filaments themselves. Mechanical studies have been conducted on all three filaments: titin (1–3), actin (4,5), and myosin (6–10). These studies (8,9) have shown that a fraction of the sarcomere's compliance arises from the extensibility of the thin and thick filaments, and not exclusively from cross-bridges, as had been supposed earlier (11). Mainly, the maximum strains reported have been in the range of 1–2% of the initial length.

In invertebrate thick filaments, however, the magnitude appears to be larger. Previous studies on isolated thick filaments from *Mytilus* and *Limulus* have shown that physiological stresses produce filament-length changes up to 23% and 66%, respectively (6). The ability to change length has been demonstrated also in synthetic vertebrate thick filaments during imposed physiological stress (10), although the magnitude was considerably smaller.

Here we report for the first time dynamic length-change measurements on isolated thick filaments. We find that isolated thick filaments from the anterior byssus retractor muscle (ABRM) of the blue mussel *Mytilus edulis* change length in steps. Steps were observed consistently, and their size was indistinguishable from that found during both contraction and stretch of intact activated sarcomeres, and of isolated activated actin-myosin filament pairs (12,13).

METHODS

Protein preparation

Native thick filaments were prepared from the ABRM of the living blue mussel, *Mytilus*, as described previously (14). Briefly, muscle was removed from the shell and placed in thick filament extraction buffer (10 mM PIPES, (pH 7.0), 8 mM Na_2ATP, 10 mM $MgCl_2$, 4 mM EGTA, 1 mM dithiothreitol (DTT)). The muscle was rinsed twice in thick filament buffer and kept in the refrigerator for ~1 h. It was diced into small pieces and homogenized twice in 7 ml of thick filament buffer in a blender (Omni Mixer, Sorvall, Newtown, CT) using the protocol 2×7 s at 1100 rpm on ice. The homogenized muscle was sedimented at 5000 *g* for 5 min. The supernatant was carefully removed and mixed with an equal volume of thick filament buffer containing 0.1% Triton X-100, and sedimented for 5 min again. Then the solution was diluted with the thick filament buffer in equal volume. The supernatant was recovered and stored on ice until used.

Solutions

The following solutions were used for preparation and experimentation. The thick filament extraction solution contained (in mM) 10 PIPES (pH 7.0), 10 $MgCl_2$, 2 EGTA, 8 ATP, and 2 DTT. The solutions used for experiments were AB buffer (pH 7.4), with a composition (in mM) of 1 EGTA, 25 imidazole, 25 KCl, 4 $MgCl_2$, and 1 DTT, and AB/BSA/GOC, with a composition of 0.5 mg/ml BSA, 3mg/ml glucose, 0.18 mg/ml glucose oxidase, 0.1 mg/ml catalase, 20 mM DTT, 1.1 mM $CaCl_2$, and 25 μM (50 μM) ATP in AB.

Apparatus

The measurement apparatus was based on a Zeiss (Oberkochen, Germany) Axiovert 135 TV microscope system (Fig. 1). The flow cell was illuminated by an intensity-adjustable QTH light source through a water-immersion condenser (Zeiss Achroplan, 63×/0.9 W). The magnified images of the three levers (see below), obtained using a 100× oil immersion objective lens and an intermediate lens (Zeiss Plan-Neofluar, 100×/1.30 oil), were projected onto an 1100-pixel photodiode array (RL1024K, EG&G, Reticon, CA). By using a standard grating of known line pairs, the calibrated magnification was found to be 99.7 nm/pixel. The time course of lever position could be recorded continuously at a pixel sampling rate of 50 kHz, which yielded a temporal resolution of 22 ms/scan, given the array length of 1100 pixels.

The specimen in the experimental chamber was attached between the tips of the stationary beam and one of the two flexible (deflectable) levers of a pair with a common base. The base was mounted on the moving tip of the piezoelectric motor, which could impose linear length changes on the specimen (15). Details of nanolevers have been described in detail in Fauver et al.

Submitted July 1, 2005, and accepted for publication August 4, 2005.

Address reprint requests to Gerald H. Pollack, Dept. of Bioengineering, University of Washington, Seattle, WA 98195. E-mail: ghp@u.washington.edu.

0006-3495/05/11/3269/08 $2.00

doi: 10.1529/biophysj.105.069864

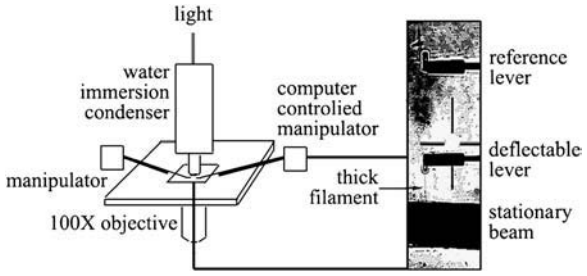

FIGURE 1 Schematic of apparatus with optical micrograph (*right*) of deflectable and reference nanolevers and stationary beam with thick filament attached. Expanded regions of levers, near tips, after magnification were projected onto the photodiode array for position measurement. The reference lever/deflectable lever pair was moved away from the stationary beam (upward direction in figure) by a computer-controlled micromanipulator to produce thick filament stretch.

(16). The above fixtures were in turn mounted on piezoelectric micromanipulators (Burleigh PCS-5000 Series patch-clamp micromanipulators, Burleigh Instruments, Victor, NY) to facilitate positioning. Before attempting to manipulate filaments, the lever pairs' position and light intensity were adjusted to optimize signal level and shape.

Experimental procedure

The stationary beam was placed in the flow cell, and 10 μl of native thick filaments was pipetted into the chamber. After ~5 min, excess thick filaments were washed away by flow of AB buffer perpendicular to the axis of the beam shafts; only a few remained in the chamber. The perpendicular flow ensured that filaments would attach largely at right angles to the reference beam axis.

Orientation and density of thick filaments attached to the nondeflectable stationary beam were examined carefully under differential interference contrast microscopy. Only filaments with a free segment projecting beyond the lever surface, and with the axis at right angles to the lever (within 90 $\pm$ 10°), were considered acceptable for experimentation. The free end of the attached filament was caught by the deflectable lever (Fig. 1).

A trial trapezoidal length change was imposed by the motor with speed ~100 $\pm$ 40 nm/s. To assure a consistently good signal, it was sometimes necessary to readjust lighting conditions so that the illumination remained uniform throughout. The stretch-release protocols were then carried out. In total, 12 thick filaments were studied.

Filament-length measurement

The photodiode array was scanned every 45 ms to produce a trace of intensity versus position of the lever tips. Filament-length change was computed as the position shift of the peak. To calculate the change of position with high resolution, an algorithm based on the minimum average risk method originally put forth by A. Kolmogorov (17) was developed (18).

The algorithm operates on repeated scans of an intensity peak, precisely quantifying peak movement from scan to scan. Because the method is differential, high resolution is achieved (19,20). The change of filament length can be computed from the relative shift between nanolever peaks. By repeating this computation for each successive scan, the time course of each peak position, and thus of filament length, could be obtained.

Step detection

Records of length change showed steps during the motor-imposed ramp as well as during creep phases. Without extensive controls we could not rule out the possibility that some of the steps seen during the phase of motor movement could have arisen from jerkiness of the motor. Also, time resolution was insufficient to provide reliable analysis of these steps. Therefore, analysis was restricted to those steps seen during the ''creep'' phase, where pauses were relatively long and motor movement ceased.

Analytical details follow largely along lines already presented for experiments on single myofibrils (12,15,19,20). To identify a step it was necessary to define a pair of pauses. The pause was taken provisionally as a segment of the trace whose estimated best fit by eye was nominally parallel to the horizontal axis. The region had to contain a minimum of five consecutive sample points to qualify; most contained more. After assigning beginning and end points of the pause, a best-fit line was computed. This fit provided a guide for slight adjustment of the break points to yield pauses with slope closest to zero. Step size was then computed as the vertical span between centers of two successive best-fit line segments. The procedure was repeated for other pauses and steps.

To avert the influence of human factors, a new step-detection algorithm based on a slope-threshold principle, was developed to identify and measure steps fully automatically (M. Wang, E. Nagornyak, and G. Pollack, unpublished). Regions of traces whose slope satisfies a near-zero criterion are taken as pauses. The slope threshold is the product of an input parameter and the overall least-square fit slope of the data, the latter computed locally along the data set with progressively increasing window size from five data points up to the desired value. Under a particular window size, consecutive least-square fits are computed by shifting by one data point each time. If the slope of the least-square fit is less than the selected slope threshold, then the least-square fit region is marked as a pause. The pause's starting and ending points are then stored in a temporary array set. Once the entire set is processed under a particular window size, the pauses in the temporary array set are compared to the pauses in the permanent array set. This procedure updates the permanent array set with newly identified pauses. It also checks for overlapping pauses: the pause with larger window size is recorded. After the data are processed with the maximum window size, each step is calculated as the vertical difference between the midpoints of consecutive pauses' least-square fits.

Postprocessing of the step data is performed by another algorithm, which queries through the recorded steps according to user-defined maximum slope and maximum deviation criteria. If either one of the two pauses used to calculate the step fails to satisfy the criteria, the step value is disregarded.

RESULTS

A representative trace of thick filament length versus time is shown in Fig. 2 (*thin black line*). Filaments generally followed the imposed trapezoidal waveform on a coarse scale (*light shaded line*), except for periods of creep immediately after each period of imposed deformation.

The thick black curve of Fig. 2 illustrates representative traces of tension versus time. Tension was calculated as the product of lever stiffness and distance change between the two tips of the flexible cantilever pair (deflectable lever and reference lever). Maximum force per filament remained within the physiological range (6). Note that the tension level after release of the thick filament is similar to the tension level before the imposed ramp. This equivalence testifies to the high stiffness of the thick filaments' connection to the levers.

Filament-length changes versus time were examined during the creep phase only (cf. Fig. 2). Within this phase, temporal resolution was adequate to track length changes with precision. Also, because the motor was stationary, any step-like fluctuations of motor-imposed lever movement

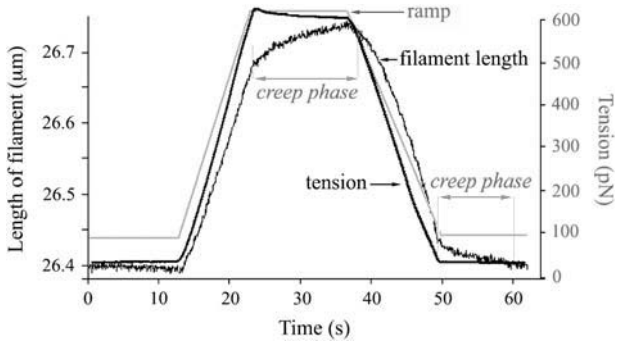

FIGURE 2 Low-resolution traces of thick-filament length change (*thin black curve*) and tension change (*thick black curve*) during motor-imposed trapezoid ramp (*light shaded curve*). Note the ''creep phase'' of filament length change, which occurs after motor movement ceases. It was during this phase that filament length changes were analyzed. Tension levels before and after stretches are similar, confirming the absence of filament slippage from the lever tips during stretch.

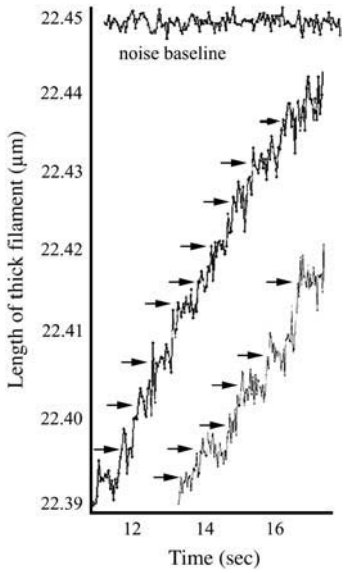

FIGURE 3 Representative traces of thick-filament length change (during creep phase), with pauses denoted by arrows. The noise level is shown on the top.

could be averted. Mean velocity during the creep phase was 9.6 ± 2.2 nm/s for lengthening and 8.8 ± 2.3 nm/s for shortening.

Steps were observed with different amplitude ramps (or levels of load). The observations were made with a mean load of 117.2 ± 93.6 pN, which corresponded to 2.4 ± 1.9 μm of length change (~13% of initial length). Sometimes, depending on ramp speed, the portion of the trace corresponding to the period of motor-imposed length change showed steps. However, the source of these steps remained somewhat vague, as there may be some contribution from motor-induced vibration. Hence, these steps were not analyzed. Only the steps observed during the subsequent creep phase, where the filament changed length more slowly, were analyzed. The creep portion of the trace was consistently staircase-like, with short pauses interspersed between steps (Fig. 3). The steps were typically 2–10 nm in size. To analyze steps, an algorithm computed the vertical spacing between successive pauses, which gave the step size. Sizes obtained from many steps were plotted as continuous histograms, two of which (including shortening and lengthening steps) are shown in Fig. 4. In both histograms, peaks are situated at approximate integer multiples of 2.7 nm. The primary peak is situated at 2.7 nm, and additional peaks are seen at 5.4 nm, 8.1 nm, and higher integer multiples of 2.7 nm.

To determine histogram-peak positions with higher precision, a Gaussian distribution was fit to each peak for all histograms; the fitted peak positions and the corresponding standard deviations are shown in Table 1. The slight shift of peaks from their ''expected'' values may have arisen from contributions from tails of the dominant neighboring peaks. Except for the higher orders, for which there were few data, peaks were generally close to their nominal values as integer multiples of 2.7 nm.

The effects of modest changes of experimental conditions were checked by varying [ATP] and [Ca^{2+}]. When activating solution was replaced by relaxing solution (low ATP, no Ca^{2+}), or by a solution with a double concentration of ATP, no step size change was detectable (Fig. 5 and Table 1).

Controls for artifact

High-resolution measurements of filament-length change are subject to various potential sources of artifact. Therefore, a series of controls was carried out.

The effect of discreteness of the photodiode array was checked in a series of experiments, when different magni-

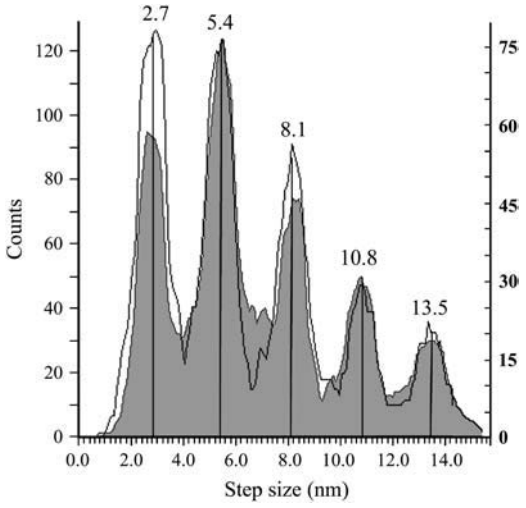

FIGURE 4 Histograms of shortening step size (*unshaded curve*, *right scale*, 435 steps) and lengthening step size (*shaded curve*, *left scale*, 830 steps) obtained during filament length change. Vertical lines indicate approximate centroids (peak values and standard deviation are shown in Table 1).

TABLE 1 Gaussian fit of peak positions

Type of histogram	Peak 1 (nm)	Peak 2 (nm)	Peak 3 (nm)	Peak 4 (nm)	Peak 5 (nm)	Peak 6 (nm)	Peak 7 (nm)	Peak 8 (nm)
Thick filament lengthening	2.75 ± 0.04	5.42 ± 0.04	8.23 ± 0.05	10.74 ± 0.07	13.71 ± 0.12			
Thick filament shortening	2.74 ± 0.05	5.26 ± 0.05	8.12 ± 0.07	10.83 ± 0.08	13.41 ± 0.10			
Solution No. 0	2.81 ± 0.11	5.31 ± 0.07	8.08 ± 0.12	10.76 ± 0.11	13.57 ± 0.12			
Solution No. 1	2.76 ± 0.04	5.35 ± 0.04	8.16 ± 0.05	10.77 ± 0.07	13.43 ± 0.09			
Solution No. 2	2.71 ± 0.05	5.36 ± 0.04	8.26 ± 0.07	10.78 ± 0.06	13.32 ± 0.09			
1.6× magnification	2.72 ± 0.05	5.24 ± 0.03	8.43 ± 0.06	10.78 ± 0.07				
Tension-traces	2.65 ± 0.08	5.43 ± 0.03	8.08 ± 0.07	10.77 ± 0.03	13.45 ± 0.04	16.24 ± 0.08	18.88 ± 0.07	
Filter	2.76 ± 0.06	5.26 ± 0.07	8.20 ± 0.07	10.71 ± 0.10	13.84 ± 0.11			
Automatic step detection	2.8 ± 0.5	5.2 ± 0.4	8.4 ± 0.5	11.0 ± 0.6				
Spider silk	6.8 ± 0.5	14.2 ± 0.8	20.8 ± 0.7	28.1 ± 0.7	34.9 ± 0.5	42.0 ± 0.4	49.2 ± 0.9	55.7 ± 0.9

fication for the photodiode array was used. To obtain higher magnification, a 1.6× slider lens was inserted, which increased overall magnification by 60%. Although noisier, traces of length change were again stepwise (Fig. 6, *inset*). The resulting steps are plotted on the histogram of Fig. 6. Although the number of data points is lower than for the standard measurements, peak locations are indistinguishable from those obtained using standard magnification (see Table 1). A second control was to test unexpected influence of motor movement. To pursue this, we measured the distance change between the two flexible levers of the lever pair instead of between one deflectable lever and the stationary beam. The two nanolevers of the pair are similarly shifted by the motor. Steps seen in this pair should be identical to those measured between the deflectable lever and the stationary beam, although the former is expected to be noisier. The resulting step-size histogram is shown in Fig. 7. Again, step size is an integer multiple of 2.7 nm (Table 1).

Another control was to restrict the data set to include only those records with relatively low noise. Thus, records in which peak-to-peak noise during the pause exceeded 3 nm were excluded. Although the number of counts decreased, the shape of the histogram did not change significantly, and step sizes remained unchanged (Fig. 8 and Table 1).

Controls were also carried out to check the method used to compute step size. Two alternatives were tried with similarly corroborative results. In the pairwise power-spectrum method (21), filament lengthening traces were reanalyzed ($n = 143$). Fig. 9 *A* shows a peak at ~2.6 nm, close to the 2.7-nm value obtained above. To check for the effects of noise, long baseline signals were acquired for each of the above traces. To each baseline was added a linear ramp at the same velocity as the respective filament-lengthening signal. Such composite signals should represent step-free lengthening, containing only noise. Fig. 9 *B* shows no distinct peak at or near 2.7 nm. Hence, noise does not appear to contribute significantly to the observed steps.

Whereas the pairwise power-spectrum method has been shown to work effectively for recurring steps of uniform size (21,22), the relative weakness of the main peak in Fig. 9 *A* implies that the method may be less suitable for irregular patterns, e.g., a step of 2.7 nm followed by a step of 4 × 2.7

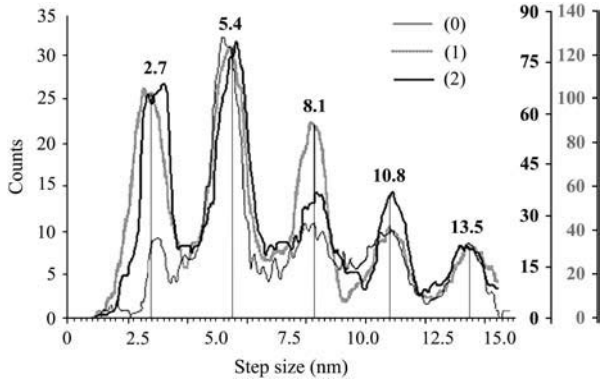

FIGURE 5 Histograms of step size obtained using different concentrations of ATP and Ca^{2+}: (0), relaxing levels of ATP, no Ca^{2+} (110 steps); (1), 25 μM ATP, 1.1 mM Ca^{2+} (787 steps); and (2), 50 μM ATP, 1.1 mM Ca^{2+} (491 steps). Vertical lines indicate approximate centroids (peak values and standard deviation are shown in Table 1).

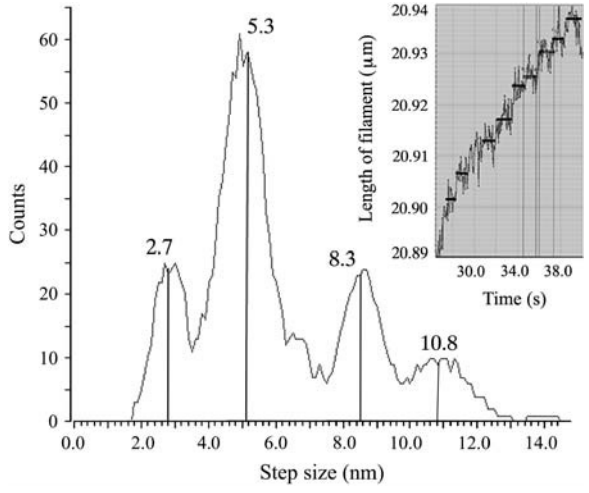

FIGURE 6 Histogram of step size obtained from measurements at higher magnification (1.6×). Computed peak locations shown at top (peak values and standard deviation are shown in Table 1). A data set of 205 steps is included, smaller than with standard magnification. (*Inset*) Representative data.

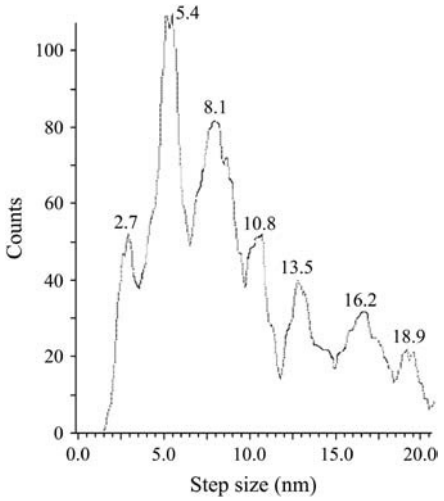

FIGURE 7 Histogram of step size obtained from traces computed from distance change between the two flexible levers of the pair (deflectable and reference levers). Histogram contains 1100 steps. Peak values and standard deviation are shown in Table 1.

nm, etc. Hence, this otherwise useful method was not pursued beyond that of testing the validity of the standard method.

A second alternative was developed to exclude any possibility of human influence on pause-step determination. In this approach an algorithm was developed to identify pauses fully automatically instead of semiautomatically (M. Wang, E. Nagornyak, and G. Pollack, unpublished). As in the current algorithm, the program defines each step by applying best-fit lines to pauses immediately before and after the step. Although resulting histogram peaks are less clear than with semiautomatic analysis, the results confirm integer multiples of 2.7 nm: peaks are seen at 2.8 nm, 5.2 nm, 8.4 nm, and 11 nm (Fig. 10 and Table 1).

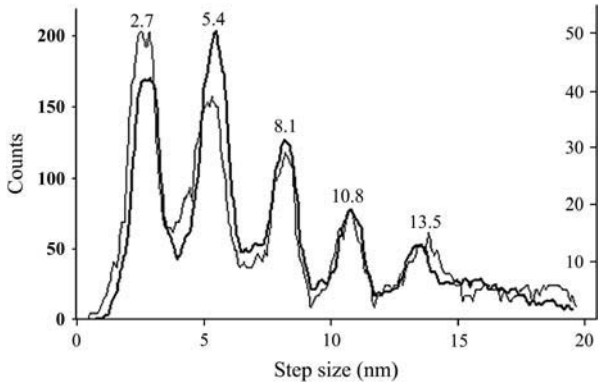

FIGURE 8 Influence of noise on step-size histograms. Bold curve contains all data points (stretch and release steps are combined). Thin curve contains only pauses with peak-to-peak noise <3 nm. The number of steps in the original histogram was 1228; in the low-noise histogram, there are 441 (peak values and standard deviation are shown in Table 1).

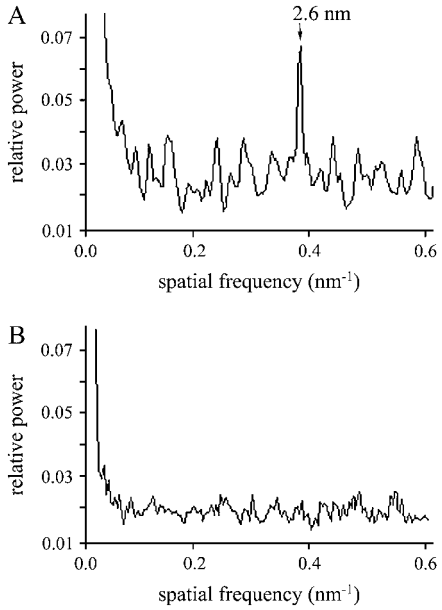

FIGURE 9 (*A*) Power spectra measured from filament lengthening records ($n = 143$ records). (*B*) Records consisting of baseline (no lengthening) plus a computer-generated ramp ($n = 44$ records). *B* shows only noise, whereas *A* shows steps at 2.6 nm.

As a final control, we examined the possibility of steps in specimens different from those in muscle. Because step size is so consistently an integer multiple of 2.7 nm, suspicion arises that the steps could originate in some unsuspected feature of the apparatus, notwithstanding the controls, above. Under experimental conditions that remained otherwise

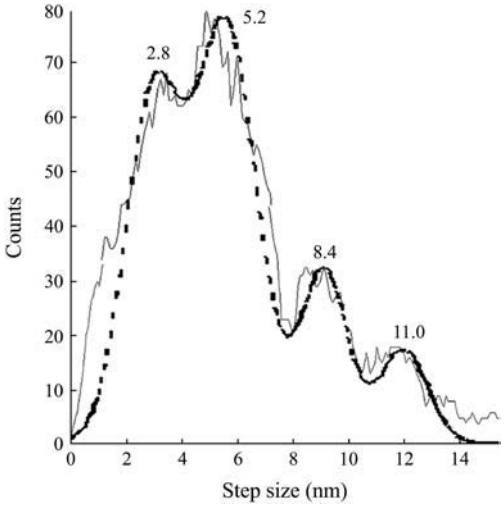

FIGURE 10 Histogram of steps from stretch-release traces (combined), computed from a fraction of original data traces using the fully automatic method (603 steps). Dashed line denotes fitted Gaussian distribution. The fitted peak positions and the corresponding standard deviations are shown in Table 1. This histogram was obtained by using the fully automatic method; all other histograms were obtained by the standard semiautomatic method.

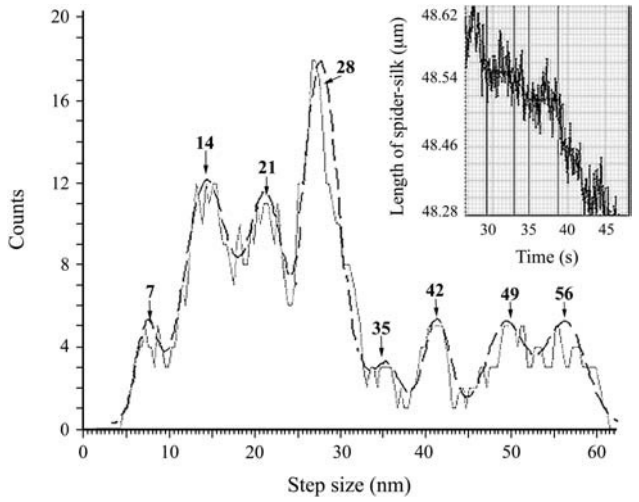

FIGURE 11 Distribution of step size obtained during stretch and release (combined) of spider silk. Peaks appear at integer multiples of 7 nm (119 steps). Inset shows a segment of the release trace. Dashed line denotes fitted Gaussian distribution, used to determine peak positions with higher precision. The fitted peak positions and the corresponding standard deviations are shown in Table 1.

identical, spider silk was substituted for the thick filament to determine whether steps of similar size (2.7 nm) might show up artifactually. Steps were observable, although less common in these specimens. The measured step size was no longer an integer multiple of 2.7 nm, but an integer multiple of ~7 nm (Fig. 11 and Table 1). A previous report on spider silk by Oroudjev at al. (23) showed steps of 14 nm. This is confirmed here as well, as the second, and relatively prominent, peak of the histogram. It appears that with the higher resolution available here, a peak corresponding to half the latter value is also seen. However, no peak at 2.7 nm or any integer multiples was detected. Hence, the possibility that the apparatus, for some unsuspected reason, consistently generates 2.7-nm steps seems remote.

DISCUSSION

We found that thick filaments of *Mytilus* were able to undergo large-magnitude, repeatable length changes within the physiological tension range, confirming the earlier report of Neumann et al. (6). The maximum physiological tension was previously estimated (6) by taking the published value of active tension per cross section and dividing by the cross-sectional density of thick filaments. Maximal contractile force per thick filament was calculated to be 12–21 nN (6). Note that *Mytilus* thick filaments are 6–50 μm long and 40–90 nm in diameter. Hence, this force is considerably larger than found in vertebrate filaments.

The current investigation has shown that the length changes occur in a stepwise manner. Steps were analyzed during the creep phases to exclude possible influence of motor vibration. Step size was found to be 2.7 nm and integer multiples thereof.

A series of controls have been carried out to check for potential sources of artifact. The effect of photodiode-array discreteness was checked by using two different magnification factors (1× and 1.6×); results were similar. The possibility of discrete events arising from ambient fluctuations was checked by analyzing traces of distance change between the pair of flexible nanolevers instead of distance between one nanolever of the pair (the deflectable lever in Fig. 1) and the stationary beam; similar steps were found. To exclude any possibility of human influence on pause-step determination, an algorithm was developed to identify pauses fully automatically instead of semiautomatically; results were similar. As an additional control, we examined the possibility of steps in specimens different from muscle. Spider silk yielded step size that was an integer multiple of ~7 nm, and this is in good agreement with AFM findings (23). Thus, all tests above were negative for artifact, and support the validity of the 2.7-nm paradigm.

The results show a high level of consistency in different situations. The step-size value was 2.7 nm and integer multiples thereof for both shortening and lengthening. This implies that the process is reversible. Also, experimental conditions did not affect the size: when concentrations of ATP and Ca^{2+} were changed within a modest range, the step-size paradigm remained consistent. Consequently, the 2.7-nm value appears to be robust—at least under the range of conditions examined. It appears to represent a basic feature of filament-length change.

In vertebrate filaments, the 2.7-nm step is an expectation of thick filament structure—predicted on the basis of charge distribution along constituent myosin rods. The thick filament cross section contains 12 rods, which splay into three ''subfilaments''. If each shortening event takes place in only one of the three subfilaments at a time, that subfilament will slide past the others. In that case, given the regular charge repeat along each myosin rod (24), the expected filament-length step is predicted to be 2.7 nm (25). The situation in invertebrates is less clear because filament backbone structure is less certain. Nevertheless, the fact that filament-length steps correspond so well to expectations from filament structure in vertebrate specimens implies the possibility of a functional role.

A hypothesis is: not only is there a single stable state of global energy minimum that corresponds to the natural length of the thick filament, but also states of local energy minima. These correspond to the pauses between steps. These minima could be created by the periodic charge distributions along the surfaces of the myosin rods. These minima are present whether the filament is being stretched or released. Although it may be obvious how the pauses could occur as the filament is actively stretched, less obvious is how the filament returns to its natural length, showing pauses

and steps as it does. There are at least two possibilities. First, because thick filaments consist not only of myosin, but also of proteins that run through the filament (the equivalent of titin in vertebrate filaments), any such proteins could provide a restoring force, which might even be spring-like. Such a force would return the filament to its natural length. A second possibility is thermal motion. If the myosin molecules are constantly fluctuating, then the most stable points will lie at the energy minima. Hence, the filament will settle at each of these minima during the return. Perhaps some combination of thermal and elastic recoil forces is the real explanation.

The possibility of thick-filament-length changes is not in conflict with x-ray diffraction data. If the filament-length change is large, one might anticipate some indication of this change on the x-ray pattern. However, if the change occurs as a one-molecule-at-a-time progression rather than uniformly among constituent molecules, then the unchanged portion of the filament will contribute to the x-ray pattern in much the same way as it does in the unshortened filament. The main myosin reflections will not change their positions, as observed. The shortened regions would contribute little to the pattern, particularly if the amount of shortening in each region were not uniform. All that would be expected in the x-ray pattern is a progressive diminution of intensity, which is observed (26,27).

This 2.7-nm paradigm appears not only in thick filaments but also in various contractile systems. The data reported by Kitamura and Yanagida using single myosin molecules translating along actin filaments showed consistent step sizes of ~5.4 nm (28,29). These values show up here as two times the primary value of 2.7 nm. Also, step sizes recently found by Liu and Pollack (13) in experiments with single actin and myosin filaments sliding past one another are integer multiples of 2.7 nm. Finally, the step size of 2.7 nm was found also in shortening and stretch of activated single myofibrillar sarcomeres, including rabbit cardiac and skeletal muscle, and insect flight muscle (12,19). Thus, three independent approaches gave the same fundamental step size.

In this regard, it is noteworthy that thick-filament-length steps follow the same 2.7-nm paradigm. Of course, this similarity could arise merely by coincidence, but in both situations the myosin filament is involved. Hence, it is possible that sarcomere length changes and thick-filament-length changes may be tied together (cf. 25,30).

In conclusion, we found substantial thick-filament-length changes, which occurred in stepwise fashion. The step size was 2.7 nm and integer multiples thereof, and did not depend on direction of length change or concentration of ATP and Ca^{2+}. Of possible relevance to the underlying contractile mechanism are the facts that: 2.7-nm length steps are anticipated from myosin-rod charge distribution, and 2.7 nm is equal to the linear repeat of actin monomers along the thin filament (30). Whether indeed thick-filament-length steps are confirmed to contribute to active contractile steps awaits the results of future work.

REFERENCES

1. Kellermayer, M. S., S. B. Smith, H. L. Granzier, and C. Bustamante. 1997. Folding-unfolding transitions in single titin molecules characterized with laser tweezers. *Science*. 276:1112–1116. Erratum appears in *Science*. 1997. 277:1117.
2. Rief, M., M. Gautel, F. Oesterhelt, J. M. Fernandez, and H. E. Gaub. 1997. Reversible unfolding of individual titin immunoglobulin domains by AFM. *Science*. 276:1109–1112.
3. Tskhovrebova, L., J. Trinick, J. A. Sleep, and R. M. Simmons. 1997. Elasticity and unfolding of single molecules of the giant muscle protein titin. *Nature*. 387:308–312.
4. Kojima, H., A. Ishijama, and T. Yanagida. 1994. Direct measurement of stiffness of single actin filaments with and without tropomyosin using in vitro nanomanipulation. *Proc. Natl. Acad. Sci. USA*. 91: 12962–12966.
5. Liu, X., and G. H. Pollack. 2002. Mechanics of F-Actin characterized with microfabricated cantilevers. *Biophys. J.* 83:2705–2715.
6. Neumann, T., M. Fauver, and G. H. Pollack. 1998. Elastic properties of isolated thick filaments measured by nanofabricated cantilevers. *Biophys. J.* 75:938–947.
7. Dewey, M. M., B. Walcott, D. E. Colflesh, H. Terry, and R. J. Levine. 1977. Changes in thick filament length in *Limulus* striated muscle. *J. Cell Biol.* 75:366–380.
8. Huxley, H. E., A. Stewart, H. Sosa, and T. Irving. 1994. X-ray diffraction measurements of the extensibility of actin and myosin filaments in contracting muscle. *Biophys. J.* 67:2411–2421.
9. Wakabayashi, K., Y. Sugimoto, H. Tanaka, Y. Ueno, Y. Takezawa, and Y. Amemiya. 1994. X-ray diffraction evidence for the extensibility of actin and myosin filaments during muscle contraction. *Biophys. J.* 67:2422–2435.
10. Dunaway, D., M. Fauver, and G. Pollack. 2002. Direct measurement of single synthetic vertebrate thick filament elasticity using nanofabricated cantilevers. *Biophys. J.* 82:3128–3133.
11. Huxley, A. F. 1974. Muscular contraction. *J. Physiol.* 243:1–43.
12. Yakovenko, O., F. Blyakhman, and G. H. Pollack. 2002. Fundamental step size in single cardiac and skeletal sarcomeres. *Am. J. Physiol. Cell Physiol.* 283:C735–C742.
13. Liu, X., and G. H. Pollack. 2004. Stepwise sliding of single actin and myosin filaments. *Biophys. J.* 86:353–358.
14. Sellers, J. R., Y. J. Han, and B. Kachar. 1991. The use of native thick filaments in in vitro motility assays. *J. Cell Sci. Suppl.* 14: 67–71.
15. Yang, P., T. Tameyasu, and G. Pollack. 1998. Stepwise dynamics of connecting filaments measured in single myofibrillar sarcomeres. *Biophys. J.* 74:1473–1483.
16. Fauver, M. E., D. L. Dunaway, H. L. Lilienfeld, H. G. Craighead, and G. H. Pollack. 1998. Microfabricated cantilevers for measurement of subcellular and molecular forces. *IEEE Trans. Biomed. Eng.* 45:891–898.
17. Kolmogorov, A. 1931. Uber die analytischen Methoden in der Wahrscheinlichkeitscrechnung. *Math. Ann.* 104:415–458.
18. Sokolov, S., A. Grinko, A. Tourovskaia, F. Reitz, O. Yakovenko, G. Pollack, and F. Blyakhman. 2003. Minimum average risk as a new peak detection algorithm applied to myofibrillar dynamics. *Comput. Methods Programs Biomed.* 72:21–26.
19. Nagornyak, E. M., F. A. Blyakhman, and G. H. Pollack. 2004. Effect of sarcomere length on step size in relaxed rabbit psoas muscle. *J. Muscle Res. Cell Motil.* 25:37–43.
20. Blyakhman, F., A. Tourovskaya, and G. Pollack. 2001. Quantal sarcomere-length changes in relaxed single myofibrils. *Biophys. J.* 81: 1093–1100.

21. Svoboda, K., C. F. Schmidt, B. J. Schnapp, and S. M. Block. 1993. Direct observation of kinesin stepping by optical trapping interferometry. *Nature*. 365:721–727.

22. Schnitzer, M. J., and S. M. Block. 1997. Kinesin hydrolyses one ATP per 8-nm step. *Nature*. 388:386–390.

23. Oroudjev, E., J. Soares, S. Arcidiacono, J. Thompson, S. Fossey, and H. Hansma. 2002. Segmented nanofibers of spider dragline silk: atomic force microscopy and single-molecule force spectroscopy. *Proc. Natl. Acad. Sci. USA*. 99(Suppl 2):6460–6465.

24. McLachlan, A. D., and J. Karn. 1982. Periodic charge distributions in the myosin rod amino acid sequence match cross-bridge spacings in muscle. *Nature*. 299:226–231.

25. Pollack, G. H. 1990. Muscles and Molecules: Uncovering the Principles of Biological Motion. Ebner and Sons, Seattle.

26. Matsubara, I., and N. Yagi. 1985. Movements of cross-bridges during and after slow length changes in active frog skeletal muscle. *J. Physiol.* 361:151–163.

27. Yagi, N., and I. Matsubara. 1984. Cross-bridge movements during slow length change of active muscle. *Biophys. J.* 45:611–614.

28. Kitamura, K., M. Tokunaga, A. H. Iwane, and T. Yanagida. 1999. A single myosin head moves along an actin filament with regular step of 5.3 nanometres. *Nature*. 397:129–134.

29. Yanagida, T., S. Esaki, A. H. Iwane, A. Ishijima, K. Kitamura, H. Tanaka, and M. Tokunaga. 2000. Single-motor mechanics and model of the myosin motor. *Philos. Trans. R. Soc. Lond. B Biol. Sci.* 355:441–447.

30. Pollack, G. H. 2001. Cell, Gels and the Engines of Life. Ebner and Sons, Seattle.